Thermoelectric generators for waste heat harvesting: A computational and experimental approach

P. Aranguren[1,2*], M. Araiz[1,2], D. Astrain[1,2], A. Martínez[1,2]

[1] *Mechanical, Energy and Materials Engineering Department Public University of Navarre, 31006 Pamplona, Spain*

[2] *Smart Cities Institute, Pamplona, Spain*

[*]*e-mail:patricia.arangureng@unavarra.es*

Keywords: thermoelectric generation; waste heat recovery; computational model; prototype

Abstract

Waste heat generation has a widespread presence into daily applications, however, due to the low-temperature grade which presents, its exploitation with the most common technologies is complicated.

Thermoelectricity presents the possibility of harvesting any temperature grade heat; besides it also includes many other advantages which make thermoelectric generators perfect for generating electric power from waste heat. A prototype divided into two levels along the chimney which uses the waste heat of a combustion has been built. The experimentation has been used to determine the parameters that influence the generation and to validate a generic computational model able to predict the thermoelectric generation of any application, but specially applications where waste heat is harvested.

The temperature and mass flow of the flue gases and the load resistance determine the generation, and consequently, these parameters have been included into the model, among many others. This computational model incorporates all the elements included into the generators (heat exchangers, ceramics, unions) and all the thermoelectric phenomena and

moreover, it takes into account the temperature loss of the flue gases while circulating along the thermoelectric generator. The built prototype presents a 65 % reduction in the generation of the two levels of the thermoelectric generator due to the temperature loss of the flue gases. The general computational model predicts the thermoelectric generation with an accuracy of the ±12 %.

Nomenclature

Symbol	**Definition**
A	Area (m^2)
$b_{\dot{W}_{TEM}}$	Systematic standard uncertainty of the thermoelectric generation
c_p	Specific heat at constant pressure (J/kgK)
D_H	Hydraulic diameter (m)
E_t	Electromotive force (V)
$h_{H,he}$	Heat transfer coefficient of the interior of the chimney (W/m^{2}K)
I	Current (A)
I_{TEM}^{i}	Current generated by the TEMs of block “i” (A)
k	Thermal conductivity (W/mK)
M_{sample}	Number of samples for each configuration
$\dot{m}_{gas}$	Mass flow of the flue gases (kg/s)
n_{blo}	Number of blocks
$Nu_{H,he}$	Nusselt number of the hot side heat exchanger
$\dot{Q}_C^{TEM}$	Heat power to dissipate by a TEM (W)
$\dot{\mathrm{Q}}_{\mathrm{Peltier}}$	Peltier heat flux (W)
$\dot{Q}_{Thomson}$	Thomson heat flux (W)
$\dot{Q}_{Joule}$	Joule heat flux (W)

$\dot{Q}_{TEM}$	Heat power that flows along the TEMs
$\dot{Q}^i$	Heat power extracted from the flue gases in block "i" (W)
$\bar{q}$	Volumetric heat generation (W/m$^{3)}$
R_L	Load resistance (Ω)
R_0	Electrical resistance of the material (Ω)
R_{CD}^i	Thermal resistance of the cold side heat dissipator of block "i" (K/W)
R_{cont}^i	Contact thermal resistance of block "i" (K/W)
R_{HD}^i	Thermal resistance of the hot side heat dissipator of block "i" (K/W)
R_{CD}^{TEM}	Thermal resistance of the cold dissipator per TEM (K/W)
R_{HD}^{TEM}	Thermal resistance of the hot dissipator per TEM (K/W)
R_{loss}^i	Thermal resistance of the heat losses through the free surface of block "i" (K/W)
R_{scr}^i	Thermal resistance of the heat losses through the bolts of block "i" (K/W)
$s_{\overline{W_{TEM}}}$	Random standard uncertainty of the mean thermoelectric generation
t	Time (s)
T_{amb}	Ambient temperature (K)
T_C^i	Temperature of the heat sink in block "i" (K)
T_C^{TEMi}	Temperature of cold side of the TEMs in block "i" (K)
T_{en}	Entry temperature of the flue gases (K)
T_{en}^i	Entry temperature of block "i" (K)
T_{ex}^i	Exit temperature of block "i" (K)
T_H^i	Temperature of the heat source in block "i" (K)
T_H^{TEMi}	Temperature of hot side of the TEMs in block "i" (K)
T_m^i	Mean temperature of block "i" (K)

T_m^{TEM}	Mean temperature of the TEMs (K)
$U_{\dot{W}_{TEM}}$	Expanded uncertainty of the thermoelectric generation
v_{gas}	Velocity of the flue gases (m/s)
V_{TEM}^i	Voltage generated by the TEMs of block “i” (V)
$\dot{W}_{aux}$	Auxiliary consumption (W)
$\dot{W}_{net}$	Net generation (W)
$\dot{W}_{TEM}$	Total thermoelectric generation (W)
$\dot{W}_{TEM}^i$	Thermoelectric generation of block “i” (W)

Greek symbols

ρ	Density (kg/m$^{3)}$
α	Seebeck coefficient (V/K)
π	Peltier coefficient (V)
σ	Thomson coefficient (V/K)
η_{TEM}	Efficiency of the TEMs
ΔT_{smoke}	Temperature difference in the flue gases (K)
ΔT_{TEM}	Temperature difference between the sides of the TEMs

Abbreviations

TEG	Thermoelectric Generator
TEM	Thermoelectric Module
TEU	Thermoelectric Unit
CFD	Computational Fluid Dynamics

1. Introduction

Severe environmental issues, such as global warming, greenhouse gases emissions, climate change, acid rain and ozone depletion, have arisen due to the excessive use of fossil resources. Hence one of the most prominent issues to face in the 21st century is to satisfy the energetic demand in an environmentally friendly manner.

Thermoelectric generation is emerging as a potential technology to help meet the goal of producing clean electric energy, due to its capacity to generate electricity from any temperature level heat. The harvesting of waste heat, a by-product heat of a process, is very convenient due to its gratuity and its widespread presence, the 40 % of the primary energy utilized in industrialized countries is emitted to the ambient as waste heat [1]. Nevertheless, most is low-temperature grade heat, explaining why its most common use is warming of fluids for heating or other purposes [2–4]. Thermoelectric generation is a promising technology for recovering low-temperature grade heat [5,6], it presents attractive characteristics such as no moving parts, modularity, reliability, robustness and maintenance free [7]. Moreover, its production of electricity is environmentally friendly [8].

The harvesting of waste heat by thermoelectric generators (TEGs) improves the efficiency of the applications and contributes to reducing fuel consumption [6]. Waste heat recovery can be widely produced: in industrial plants, power plants, waste incineration plants, vehicles, aircraft, helicopters, marine vessels and so on [9,10]. Below are presented some key findings for different types of waste heat recovery applications. A TEG comprised of four thermoelectric modules (TEMs) was built for a pellet boiler obtaining a maximum power output of 8.5 W at a temperature difference of 112.8 ºC and achieving self-sufficient operation of the combustion and heating system [11]. The waste heat harvesting of a diesel engine by a TEG formed by 40 TEMs produced a maximum power output of 119 W, with a maximum energy conversion efficiency of 2.8 % [12]. A 1kW TEG using the 95 ^{o}C spring water of Tohoku district obtained a total energy generation of 1927 kWh [13]. A 10 kW class grid connected TEG system for JFE’s continuous casting line was implemented with a total of 896 TEMs, which generated power using radiant heat [14]. A thermoelectric power density of 259 W/m^2 was obtained recovering waste heat from a paper mill’s combustion boiler using TEGs provided with thermosyphons [15]. The objective of improving a 5 % the fuel economy of light-duty and/or personal automobiles by the use of TEG is nowadays is widely studied [16,17]. Some are the approaches: researching on the non-uniformity of the temperature difference across thermoelectric units along the streamwise direction [18], evaluating the weight penalty incurred when a TEG is located at the vehicle [19] and studying interior inserts to enhance thermal transfer but not negatively influence the back pressure [20] among others.

The experimental setups are not very common in the literature, most of the studies are referred to mathematical models able to simulate the behavior of the TEGs. Nevertheless, the computational models need to bear in mind all the thermoelectric effects, the dependence of the temperature on the properties and effects, and each of the element present in the system (including the heat exchangers, the contacts, the ceramics of the TEMs ...) [21–23]. Moreover, for those cases where the waste heat is scavenged, the temperature decrease of the flue gases must be taken into account to obtain accurate results, due to the big difference between the entry and exit temperatures that they experiment while flowing through the TEG [24]. Due to the low efficiency that the TEGs present [25,26], great amounts of energy are needed in these applications, resulting in a big temperature decrease that needs to be accounted for.

This study presents a novel computational model that accurately simulates the behavior of TEGs which harvest waste heat. It includes the temperature drop of the flue gases while they flow across the TEG, a very important variable to consider taking into account that the temperature difference between the entry and exit can be very considerable. Besides, this research includes a TEG that has been designed, built and experimentally tested to be located at the exhaust of a combustion chamber. The experimentation includes different parameters which influence the generation, such as the temperature and mass flow of the flue gases and the load resistances, parameters that have been included in the computational simulation.

2. Methodology and computational model

The computational model includes each of the thermoelectric phenomena (the Peltier, Seebeck, Thomson and Joule effects), it incorporates the totality of the elements included into the TEG (heat exchangers, ceramic plates, unions, screws, thermoelectric material...) and the properties of the materials are a function of the temperature. Moreover, it solves the transient state, and it incorporates the temperature drop of the flue gases, a very important parameter to take into account in waste heat harvesting applications.

To consider the temperature drop of the flue gases the direction in which the gases flow has been discretized into some blocks (n_{blo}), as it can be seen in Figure 1. Within each block, the temperature of the flue gases is obtained as the mean temperature between the entry and exit temperatures of the gases in the block ($T_m^i = 1/2(T_{en}^i + T_{ex}^i)$). This temperature is considered as the temperature of the heat source $T_H^i = T_m^i$ of the block while the temperature of the heat sink is defined as T_C^i. As the blocks are defined one following the previous one, the entry temperature of a block corresponds with the exit temperature of the previous one, $T_{en}^i = T_{ex}^{i-1}$.

Each of the thermoelectric phenomena (Eq. (1)-(4)) along with the Fourier law (Eq. (5)) are solved for each block to obtain the thermoelectric generation.

$$\alpha_{AB} = \frac{dE_t}{dT} = \alpha_A - \alpha_B \tag{1}$$

$$\dot{Q}_{\mathrm{Peltier}} = \pm \pi_{AB} I = \pm IT(\alpha_A - \alpha_B) \tag{2}$$

$$\dot{Q}_{Thomson} = -\sigma \vec{I}(\overrightarrow{\Delta T}) \tag{3}$$

$$\dot{Q}_{Joule} = R_0 I^2 \tag{4}$$

$$\rho c_p \frac{\delta T}{\delta t} = k\left(\frac{\delta^2 T}{\delta x_2} + \frac{\delta^2 T}{\delta y_2} + \frac{\delta^2 T}{\delta z_2}\right) + \bar{q} \tag{5}$$

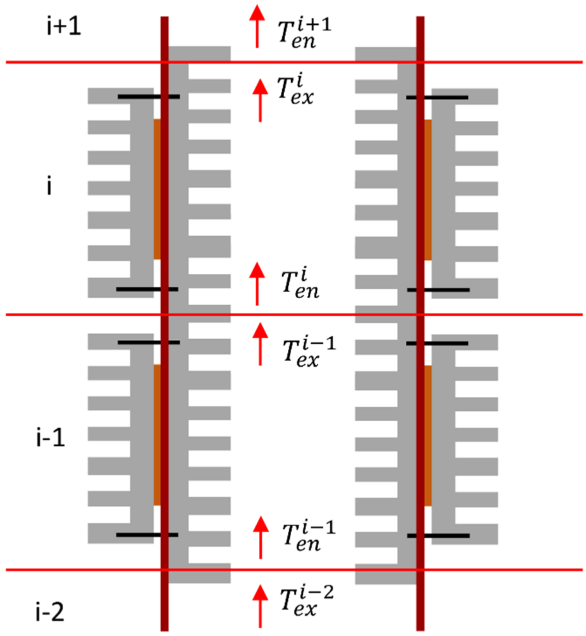

Figure 1. Discretization of the pipe into blocks to account for the temperature loss of the flue gases

Within the block, the thermal and electric phenomena are solved using the finite difference method, due to the complicated differential system that has to be solved. Consequently, the TEG of each block is discretized into 16 nodes, as Figure 2 depicts. All the elements present in a TEG are present into the discretization, including the heat exchangers located on both sides of the TEMs, the ceramic plates that conform the modules, the electrical unions of thermoelectric materials, the thermoelectric material and the screws needed to ensure good contact between the elements. The heat source is reproduced in node 1 while the heat sink in node 16. The hot and cold side heat exchangers are defined by nodes 2 and 15 respectively. Finally, the TEMs are represented by 12 nodes, from node 3 to node 14, being node 3 the hot ceramic plate which represents the temperature of the hot side of the TEM (T_H^{TEMi}), nodes 4-13 the thermoelectric material and the unions and node 14 the cold ceramic plate of the TEMs (T_C^{TEMi}).

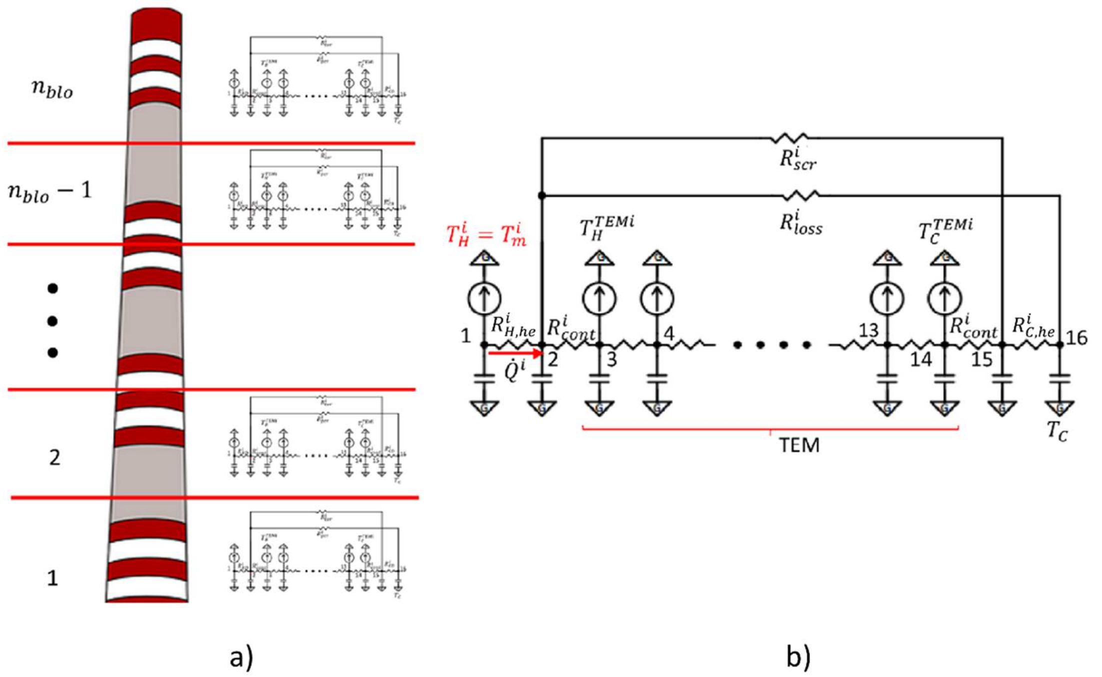

Figure 2. Discretization the system, a) Discretization into blocks of the chimney, b) Discretization into nodes of the TEG of a block and its electrical analogy

The different elements of the TEG are represented by thermal resistances and heat capacities [23,27]. $R_{H,he}^i$ and $R_{C,he}^i$ stand for the thermal resistances of the hot and cold side heat exchangers respectively. R_{cont}^i is the contact thermal resistances. R_{loss}^i and R_{scr}^i represent the alternative path that the heat flux can follow to reach the heat sink. Solely the heat that crosses the TEMs can be transformed into electric power, thus the heat that reaches the heat sink without going across the modules is wasted. R_{loss}^{i} stands for the thermal resistance of the heat losses that happen through the wall of the pipe which conducts the flue gases, while R_{scr}^{i} stands for the resistance of the screws which secure good contact between the TEMs and the heat exchangers located on both sides of them. Figure 3 presents the heat fluxes that could exist from the heat source (the flue gases) to the cold sink (the ambient).

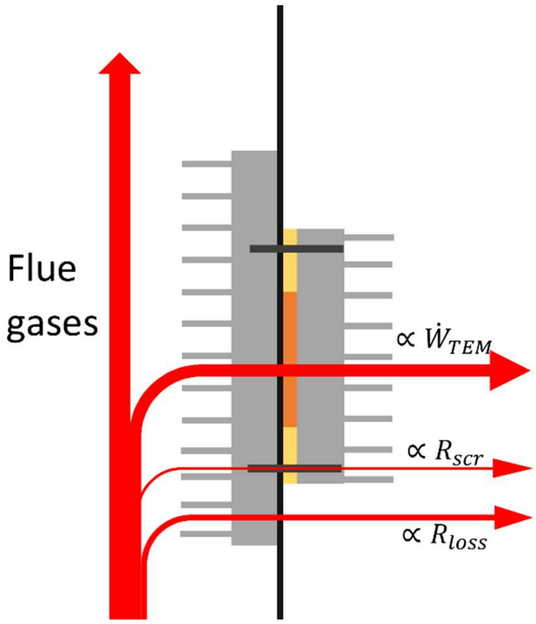

Figure 3. Heat fluxes that leave the flue gases to reach the cold sink

The computational model starts from the first block using the temperature of the application as the entry temperature of the block. As the exit temperature is not known, the mean temperature cannot be computed, hence, in a first instance, the mean temperature is matched with the entry temperature. The finite difference method solves the phenomena involved in the thermoelectric generation and obtains the temperatures of the nodes of the TEG, the heat fluxes that flow along the different paths and the thermoelectric generation. The heat flux that is absorbed from the flue gases ($\dot{Q}^{i}$) is used to compute the temperature drop of the gases in block “i”. This heat is included into Eq. (6), where $\dot{m}_{gas}$ is the mass flow of the flue gases and c_p their specific heat, to obtain the exit temperature of the flue gases. Then, the mean temperature is computed and compared with the previous iteration to state whether the iteration loop should continue or not. The tolerance is stipulated by the user, a comprehensive value could be 0.1 ºC, as the computational time is not high and the model could supply accurate results.

$$T_{ex}^{i} = T_{en}^{i} - \frac{\dot{Q}^{i}}{\dot{m}_{gas} c_p} \quad (6)$$

Once the first block is solved, the exit temperature of that block corresponds to the entry temperature of the second block, the necessary input to continue the calculation until the exit temperature of the application (the exit temperature of the last block) is computed. The thermoelectric generation is obtained adding the thermoelectric generations of each block ($\dot{W}_{TEM} = \sum_{i=1}^{i=n_{blo}} \dot{W}_{TEM}^{i}$). Figure 4 presents the methodology of calculation of the computational model.

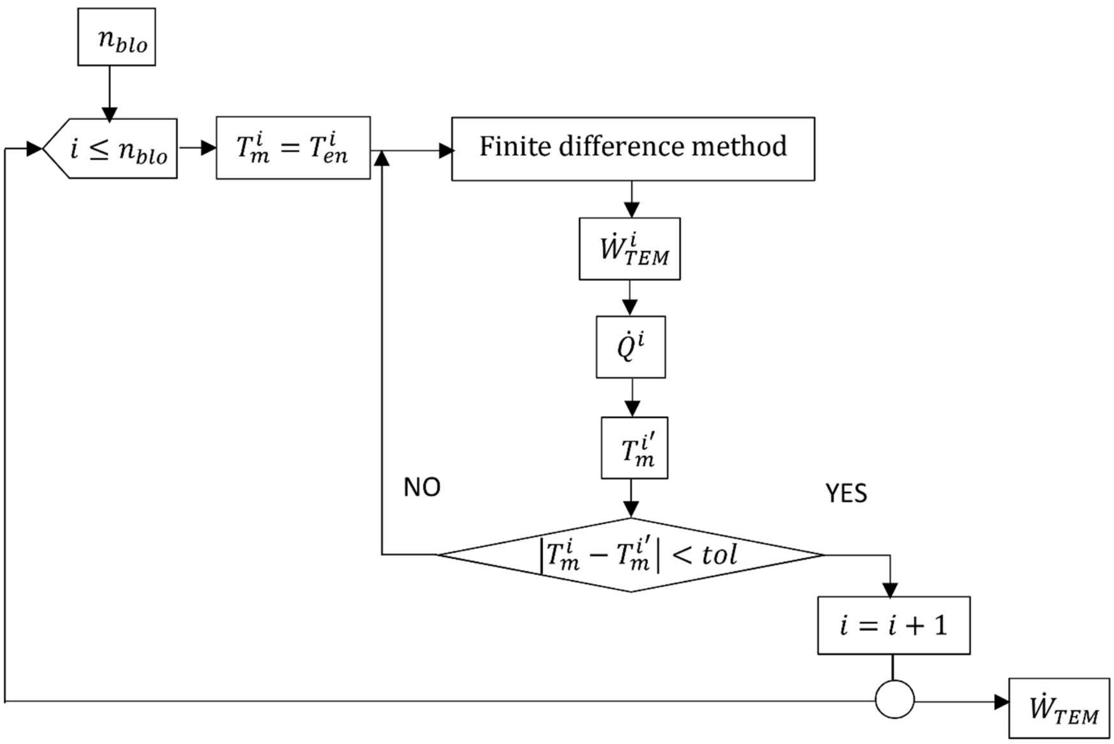

Figure 4. Scheme of the resolution methodology of the computational model

3. Prototype description and experimentation

A TEG has been designed and built to be located at the exhaust of a combustion chamber. The prototype harvests the waste heat of the flue gases of the chamber and obtains electric energy thanks to the Seebeck effect. This prototype has been designed to validate the previous described computational model. The interior of the duct by which flue gases circulate presents flat surfaces, and on the exterior of the duct, the cold side of the TEMs, finned dissipators provided with fans to make air circulate through their fins are located. The whole application is presented in Figure 5.

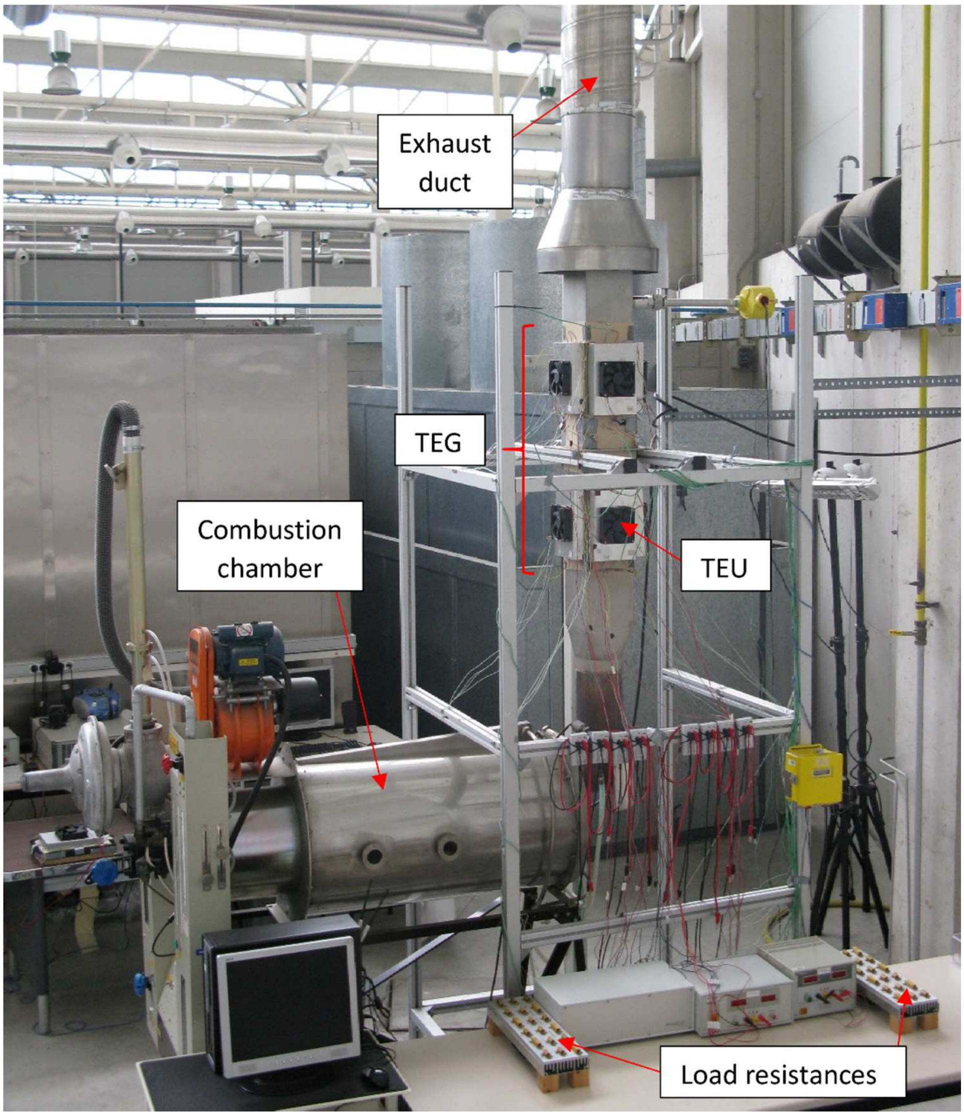

Figure 5. TEG located at the exhaust of the combustion chamber

a. Prototype description

The prototype is located at the exhaust of a combustion chamber. The combustion chamber is used to warm water up. The mass flow of the fuel (natural gas), as well as the mass flow of the air, can be modified to get the different mass flow and temperature of the flue gases to obtain different scenarios for the experimentation and the validation of the computational model.

The TEG is composed by 32 TEMs disposed of in two levels which cover all the faces of the TEG. The 32 TEMs are Marlow TG12-8-01L [28] 40 x 40 mm^2 and are specially manufactured to endure up to 230 ^{0}C on their hot side. The temperature dependent properties of the modules can be found in [23].

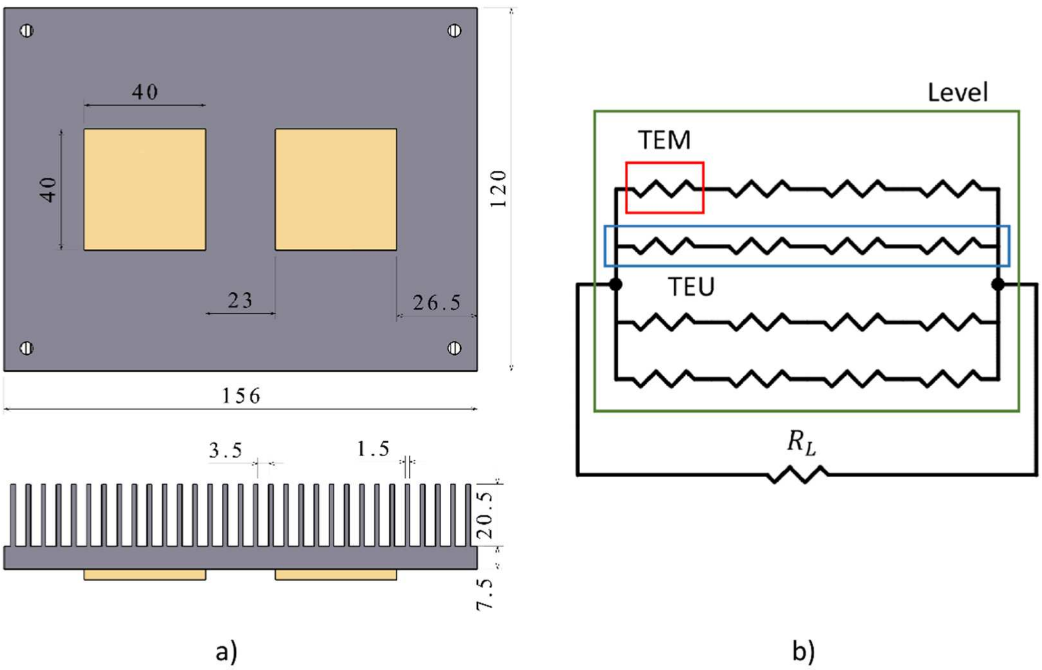

Figure 6. TEU characteristics, a) one dissipator of the thermoelectric unit with the two TEMs, b) schematic of the electrical connection.

To place the TEGs, the transversal area of the TEG presents an external dimension of 177 x 177 mm^2. Each of the levels is composed by 16 TEMs distributed into 4 thermoelectric units (TEUs), each one of them located on one side of the TEG. The TEUs are formed by two finned dissipators placed one followed by the other, and four TEMs two on each dissipator, as Figure 6 a) shows. The modules of the same TEU are electrically connected in series while the TEUs of the same level are connected in parallel, as figure 6 b) depicts. The two levels are not electrically connected. Hence each level is connected to its load resistance, obtaining the thermoelectric generation of the level.

The reason to have two dissipators instead of a bigger one stays behind an easier assembly process, securing smaller contact thermal resistances. The finned dissipators present a fin spacing of 3.5 mm, a fin thickness of 1.5 mm, a fin height of 20.5 mm and a base thickness of 7.5 mm, as Figure 6 a) depicts. There is a wind tunnel provided with a fan which covers both dissipators of the TEU, as it can be seen in Figure 5. The fans are Sunon MEC0251V1 with dimensions 120 x 120 mm^2 and a maximum power consumption of 5.4 W and they prevent the TEG from getting damaged.

The prototype is provided with temperature and mass flow sensors to monitor the properties of each test. In total there are 34 surface temperature probes, 16 sensors located on the hot side of the TEMs (T_{Hx}), 16 located on the cold side (T_{Cx}) and 2 located on the exterior wall of the TEG at the exit and entry of the first and second levels respectively (T_{supx}). Two more temperature probes save the temperature of the ambient (T_{ambx}). The previously mentioned temperature sensors are K type thermocouples with a resolution of 0.1 ^{0}C and an accuracy of ±0.5 ^{0}C. To measure the temperature of the flue gases there are 10 K type thermocouples able to measure up to 1100 ^{0}C. Their resolution and accuracy are 0.1 and ±0.5 ^{0}C respectively. They are located at the entry and exit of the lower and upper level, as Figure 7 presents. A thermal mass flow meter provided with a temperature sensor obtains the mass flow of the flue gases, the resolution is 0.1 kg/h and 0.1 ^{0}C for the mass flow and the temperature respectively and its accuracy is indicated in Table 1. To obtain the electric power generated, the prototype is provided with 2 ammeters and 2 voltmeters. The ammeters resolution and accuracy are 0.01 and ±0.02 A, while the voltmeters resolution and accuracy are 0.1 and ±0.4 V respectively. The accuracy values of the different probes present in Table 1 correspond to the systematic standard uncertainties of the directly measured parameters (temperature, voltage, current and mass flow). Their random standard uncertainties obtained from the experimentation are also included in Table 1. Figure 7 presents the measurement probes and the location of all of them.

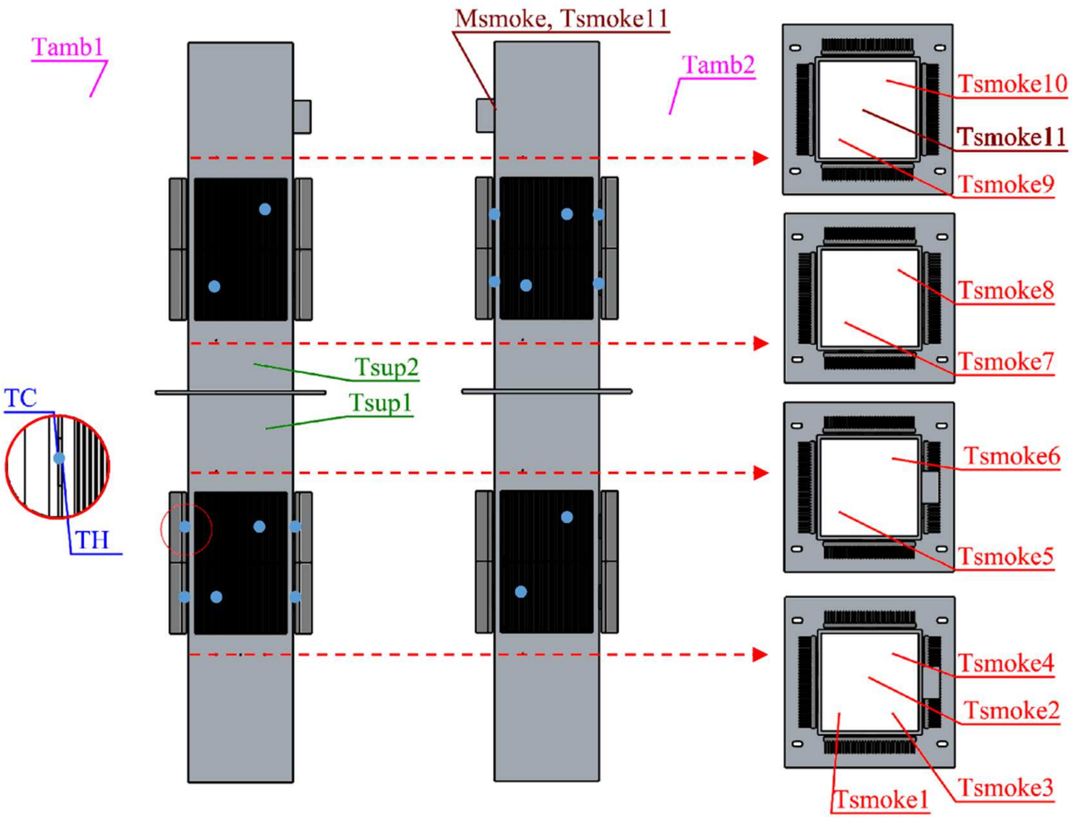

Figure 7. Measurement probes present at the TEG

The electric power obtained from the TEG depends on the load resistance connected [29]. To get the maximum power generation, two stacks with easily connected fixed resistances have been designed in order to connect variable resistances to each level of the TEG to get the optimal power generation.

Sensor	Resolution	Accuracy // Systematic random uncertainty	Random standard uncertainty
Surface temperature (^{o}C)	0.1	±0.5	3.45
Flue gas temperature (^{o}C)	0.1	±0.5	1.50
Mass flow meter (kg/h)	0.1	±1 % measured value + 0.5 % full scale	2.26
Mass flow meter (^{o}C)	0.1	±1.2	2.53
Ammeter (A)	0.01	±0.02	0.052
Voltmeter (V)	0.1	±0.4	0.0057

Table 1. Resolution and accuracy of the measurement probes

b. Prototype experimentation

Modifying the mass flow of the natural gas and the air, different conditions of temperature and mass flow of the flue gases can be obtained. The optimal thermoelectric generation as a function of the temperature and mass flow of the flue gases and the power consumption of the fans has been obtained.

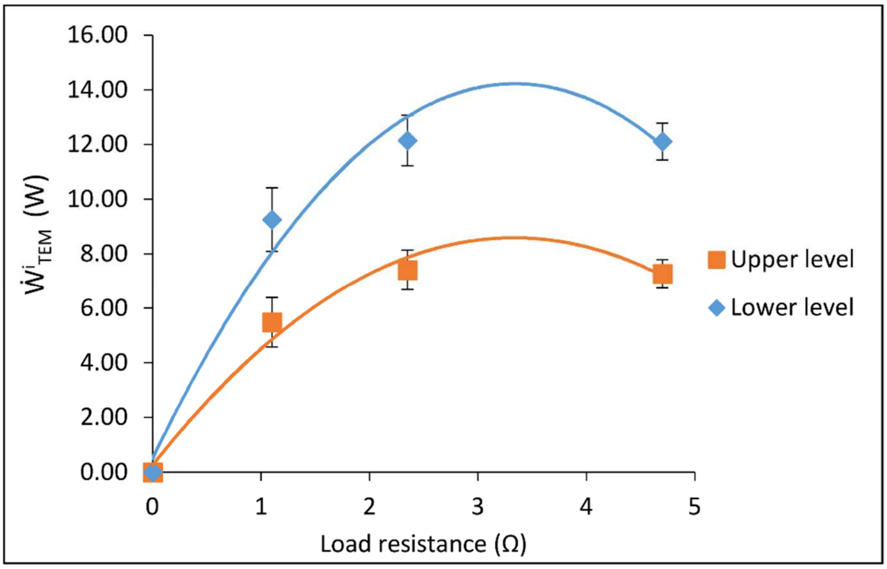

Figure 8. Influence of the load resistance on the thermoelectric generation for a mass flow of 133 kg/h and a temperature inlet of 525 ^{0}C.

To get the maximum thermoelectric generation at each working conditions, the load resistance has to be varied. Figure 8 shows the influence of the load resistance on the thermoelectric generation of the lower and upper levels with a mass flow of the flue gases of 133 kg/h and a temperature at the entry of the TEG of 525 ^{0}C. This plot also presents the expanded uncertainty of the measured values. The fitting curve fits within the error bars in both cases, for the upper and lower generations. The entry temperature (T_{en}) has been computed as the arithmetic average between the temperature probes that are located at the entry of the level ($Tsmoke1, Tsmoke2, Tsmoke3\ and\ Tsmoke4$).

Figure 8 presents the influence of the temperature loss of the flue gases. The upper level modules produce less electric power because the temperature of the flue gases at the entry of the upper level is lower than at the entry of the TEG. The optimal generation at the lower level is $\dot{W}^1_{TEM} = 14.15$ W while the one for the upper level is $\dot{W}^2_{TEM} = 8.6$ W, so the lower level presents a 65 % more power production than the upper level. The load resistance that obtains the optimal power per level, in both cases is $R_L = 3.4\ \Omega$. The maximum generation is obtained when the load resistance matches the internal resistance of the device [30]. In this case, the resistance approximately corresponds with the manufacturer's provided value [28].

To study the influence of the temperature and the mass flow of the flue gases on the thermoelectric generation nine experiments combining three entry temperatures ($T_{en} = 490, 525$ and 560 ^{o}C) of the flue gases and three mass flows ($\dot{m}_{gas} = 100, 130$ and 170 kg/h) were performed. The optimal thermoelectric generation obtained by the lower and upper levels as a function of the temperature and mass flow of the flue gases is present in Figure 9. The lower level generation is present in Figure 9 a). The maximum thermoelectric generation corresponds to 17.6 W obtained with the biggest temperature and mass flow. The increase of the temperature of the flue gases is deterrent, the rise of the temperature from 525 to 560 ºC, at a mass flow of 170 kg/h, obtains an increment on the generation of the 11 %. Figure 9 b) presents the optimal generation of the upper level of the TEG. Once more the temperature influence is palpable, the generation from the upper level is noticeably lower as it can be seen in Figure 9. The influence of the mass flow of the gases is also depicted, increasing the mass flow from 133 to 170 kg/h at a temperature of 560 ºC, the generation grows a 6 %.

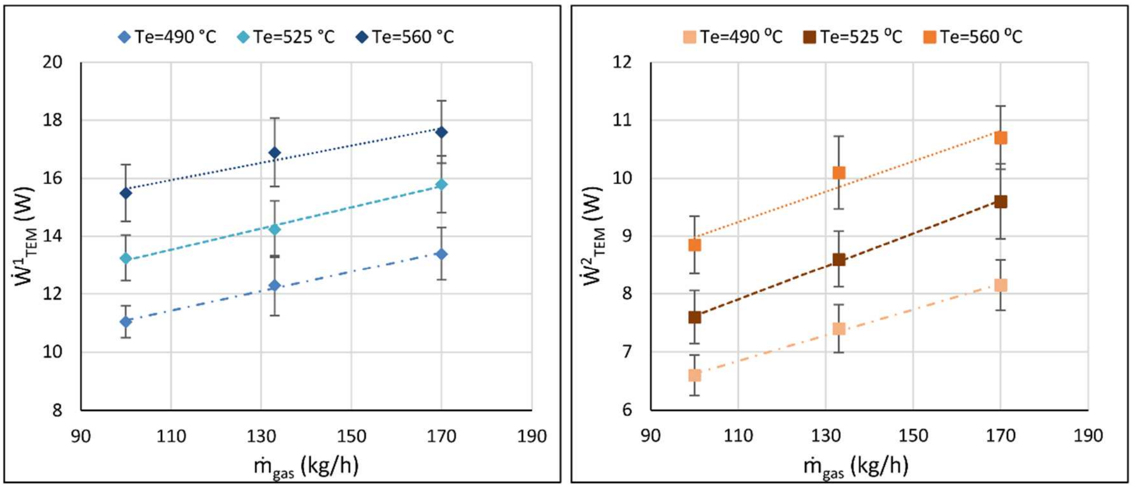

a) b)

Figure 9. Optimal thermoelectric generation as a function of the temperature and mass flow of the flue gases, a) lower level, b) upper level

Each TEU presents a fan in order to make air circulate through their fins and improve the thermal resistance of the heat exchangers located on the cold side of the TEMs. The power supplied to the fans has been modified to study its influence on the thermoelectric and net generation. The net generation is computed as the thermoelectric generation minus the consumption of the auxiliary equipment ($\dot{W}_{net} = \dot{W}_{TEM} - \dot{W}_{aux}$). In this application, the consumption of the auxiliary equipment corresponds with the power supplied to the fans in charge of producing forced convection at the heat exchangers of the cold side. Figure 10 displays the thermoelectric and net generation of the TEG as a function of the voltage supplied to the fans. As the figure shows, the thermoelectric generation grows along with the auxiliary consumption because the thermal resistances of the heat exchangers located on the cold sides improve, obtaining a greater temperature difference on the faces of the TEMs and thus obtaining a higher generation. The optimal net generation corresponds to the smallest auxiliary consumption studied, because the consumption of the auxiliary equipment grows to a greater extent than the thermoelectric generation. The net generation is the important parameter to optimize, because it is the real energy that can be used at an application, hence, the scenarios where the net generation is negative are not desirable, because instead of generating the TEG is consuming energy. In this case, the voltage input of 4 V corresponds with the minimum voltage that can be applied to the fans to make them rotate. Although it could seem that a scenario without fans could be desirable, for this particular case it is not an option because the spacing between fins is very small and thus forced convection is needed.

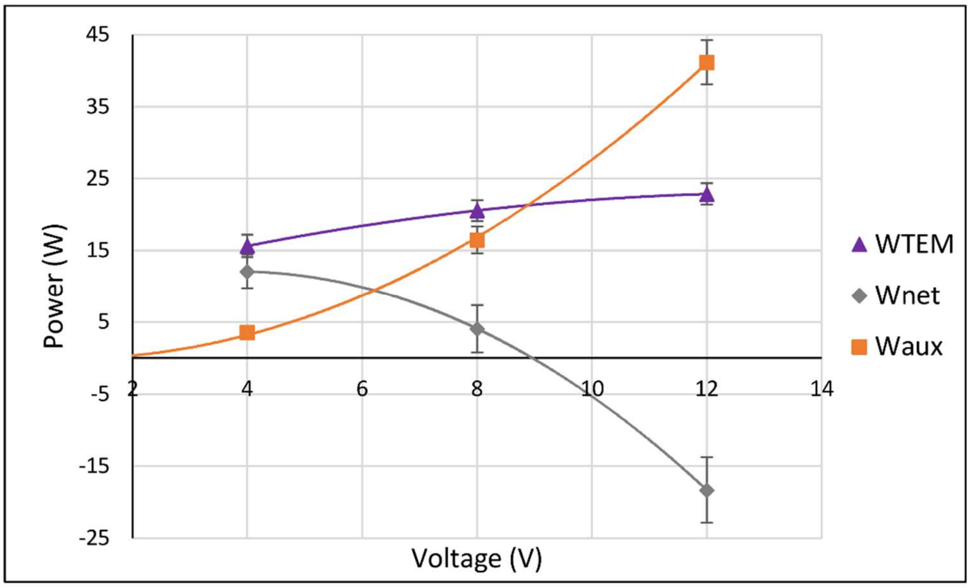

Figure 10. Thermoelectric and net generation of the TEG as a function of the voltage supplied to the fans for an entry temperature of $T_{en} = 525\ ^0C$ and a mass flow of $\dot{m}_{gas} = 133\ kg/h$ for the flue gases.

4. Validation methodology

The computational model obtains the thermoelectric generation of any application. However, it has been specially designed for waste heat harvesting applications, including the temperature loss of the flue gases while they flow along the TEG. The model includes each of the elements present in the TEG. Thus the heat exchangers located on both sides of the TEMs and the contact resistances have to be thermally characterized and included into the model. Moreover, the data of the TEMs is included through their temperature dependent properties [23].

a. Thermal resistance of the hot side

To obtain the thermal resistance between the heat source and the hot side of the TEMs a fluid dynamics software (CFD) has been used, ANSYS Fluent. In the interior of the chimney, there is no heat exchanger to help the heat transmission; the interior walls are the only areas that exchange heat with the TEMs. The thermal resistance per TEM has been obtained as a function of the velocity of the flue gases and their temperature, as Eq. (7)-(9) present. Eq. (7) includes the dimensionless Nusselt number used to compute the thermal resistance per TEM of the heat exchanger of the hot side ($R_{H,he}^{TEM}$). The heat transfer coefficient ($h_{H,he}$) is obtained through the Nusselt number, the hydraulic diameter of the chimney (D_H) and the thermal conductivity of the flue gases (k), Eq. (8). To compute the thermal resistance of the hot side, the corresponding area of a TEM at the chimney is used (63 x 90 mm^2), as Eq. (9) shows. The Nusselt expression used to represent the heat transfer in the interior of the chimney presents a $R^2 = 98$ %.

$$Nu_{H,he} = 0.9595 Re^{0.7395} Pr^{-0.2193} \tag{7}$$

$$Nu_{H,he} = \frac{h_{H,he} D_H}{k} \tag{8}$$

$$R_{H,he}^{TEM} = \frac{1}{h_{H,he} A} \tag{9}$$

To obtain the previous expression the geometry of the chimney has been included into the software and later meshed. The mesh can be found in Figure 11 a), it is fine enough to correctly represent the velocity and temperature boundary layers of the flue gases, as a grid independence study previously conducted showed. The boundary conditions used are velocity inlet, to include the velocity and temperature of the flue gases, pressure outlet to state the exit of the gases, walls for the walls of the chimney, differentiating between the adiabatic zones and the zones covered by TEMs and double symmetry not to represent the whole chimney, but a quarter. Besides, the geometry of the whole chimney has been taken into account adding the diffusor that converts the cylindrical shape of the chimney into quadrangular cross section to accommodate the TEMs.

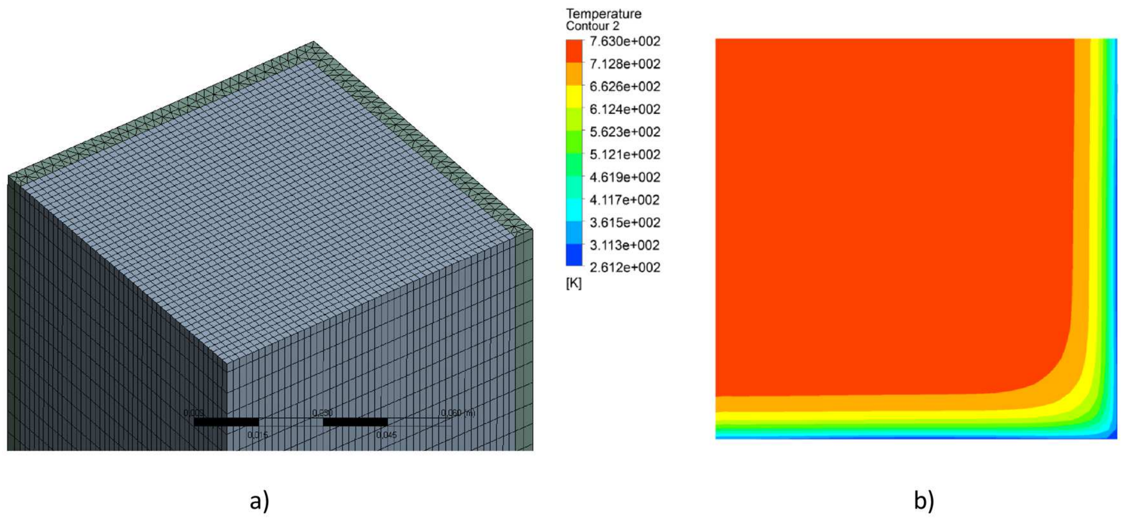

Figure 11. Computational simulation, a) mesh, b) temperature contours of the flue gases

b. Thermal resistance of the heat exchanger of the cold side

To obtain the thermal resistance of the finned dissipators located on the cold side, a TEU was tested, two heat exchangers with two TEMs each and a wind tunnel provided with a fan, as Figure 12a) presents. Four electrical resistances were used to simulate the heat used to thermally characterize the dissipators. The electrical resistances are located at the same place as the TEMs are at the TEG. On the opposite side of the dissipators, isolation can be found to secure that all the heat that is produced by the electrical resistances reaches the finned dissipators.

The finned dissipators have been characterized as a function of the supplied voltage to the fans, as Figure 12 b) presents. To decrease the experimental uncertainty three replicas of each voltage supply have been made. To obtain the resistance per TEM Eq. (10) has been used.

$$R_{C,he}^{TEM} = \frac{T_m^{TEM} - T_{amb}}{\dot{Q}_C^{TEM}} \tag{10}$$

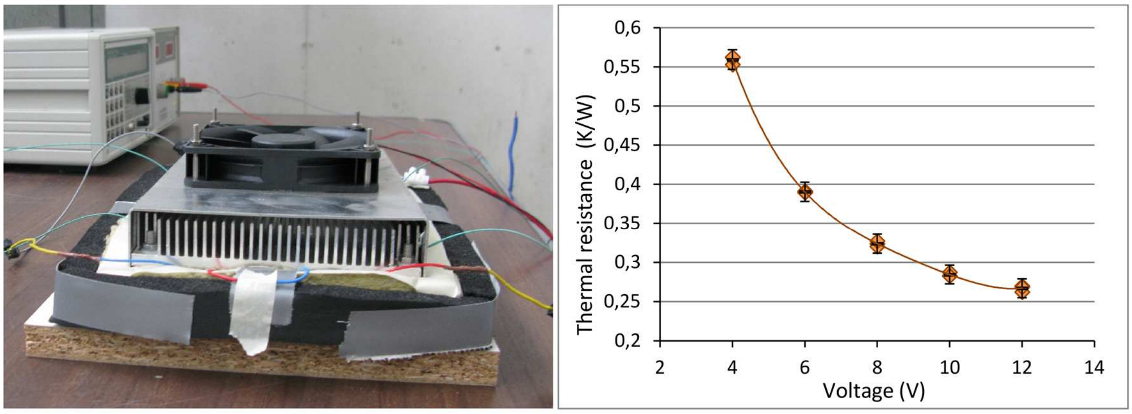

a) b)

Figure 12. Thermal characterization of the finned dissipators, a) thermal resistance as a function of the voltage supplied to the fans, b) assembly of the tests

c. Parameters fitting

The contact resistances are inherent to each assembly. The ideal would be to have negligible contact resistances which do not influence the thermoelectric generation, but sadly they have to be taken into account to compute the generation. To measure the contact resistances 9 open circuit tests were performed varying the temperature and mass flow of the flue gases. The absence of current through the thermoelectric material procures no thermoelectric effects, and thus the contact resistances can be easily computed using the computational model and the experimental values. The open circuit voltage is computationally obtained, and the temperature differences between the two sides of the TEMs are compared to obtain the contact resistances using the calorific power that crosses the modules. The contact resistance of each TEU on each side of the modules has been computed to obtain the average value for each level of the TEG. The lower level presents a resistance per TEM of $R_{cont}^{TEM} = 0.1214\ K/W$ while the upper level resistance is $R_{cont}^{TEM} = 0.1355\ K/W$.

The thermal resistances that represent the alternative paths that can follow the heat to reach the heat sink, R_{loss}^{i} and R_{scr}^{i}, have been defined as the sum of conductive, convective and contact resistances. The conduction is defined through the isolating material which presents a thermal conductivity of 0.15 W/mK and a thickness of 3 or 3.5 mm. The convective resistance is obtained with a typical natural convection coefficient (h=6 W/m^{2}K) [31].

d. Results

The thermoelectric power generation is the parameter used to evaluate the performance of the TEGs. The maximum standard random uncertainty of the thermoelectric generation is calculated using three replicas of one of the experimentations ($T_{en} = 525\ ^0C$, $\dot{m}_{gas} = 133 kg/h$) through Eq. (14)-(15) [32], which depends on the number of replicas, in this case $M_{sample} = 3$. The replicas were performed in different days, switching off and on the combustion chamber and fitting the parameters to obtain the same mass flow and temperature of the flue gases, while modifying the load resistances to the three studied cases (1.1, 2.3 and 4.7 Ω) . The expanded uncertainty (Eq. (12)) is obtained adding the maximum standard systematic uncertainty of the experiments and the maximum standard random uncertainty obtained from the three replicas of the experiment ($T_{en} = 525\ ^0C$, $\dot{m}_{gas} = 133 kg/h$). The thermoelectric generation of each level is calculated multiplying the current and voltage (I^{i}_{TEM} and V^{i}_{TEM} respectively), hence the standard systematic uncertainty can be calculated using Eq. (13), which includes the accuracy of the voltmeters and ammeters used, Table 1.

$$\dot{W}_{TEM} = V^{1}_{TEM} I^{1}_{TEM} + V^{2}_{TEM} I^{2}_{TEM} \tag{11}$$

$$U_{\dot{W}_{TEM}} = 2\left(b^{2}_{\dot{W}_{TEM}} + s^{2}_{\overline{\dot{W}_{TEM}}}\right)^{\frac{1}{2}} \tag{12}$$

$$b^{2}_{\dot{W}_{TEM}} = \left(\frac{\partial \dot{W}_{TEM}}{\partial V^{1}_{TEM}}\right)^{2} b^{2}_{V^{1}_{TEM}} + \left(\frac{\partial \dot{W}_{TEM}}{\partial I^{1}_{TEM}}\right)^{2} b^{2}_{I^{1}_{TEM}} + \left(\frac{\partial \dot{W}_{TEM}}{\partial V^{2}_{TEM}}\right)^{2} b^{2}_{V^{2}_{TEM}} + \left(\frac{\partial \dot{W}_{TEM}}{\partial I^{2}_{TEM}}\right)^{2} b^{2}_{I^{2}_{TEM}} \tag{13}$$

$$s^{2}_{\overline{\dot{W}_{TEM}}} = \frac{1}{M_{sample}\left(M_{sample} - 1\right)} \sum_{k=1}^{M_{sample}} \left(\dot{W}_{TEM,k} - \overline{\dot{W}_{TEM}}\right)^{2} \tag{14}$$

$$\overline{\dot{W}_{TEM}} = \frac{1}{M_{sample}} \sum_{k=1}^{M_{sample}} \dot{W}_{TEM,k} \tag{15}$$

Table 2 presents the computational and experimental results obtained. The generated power and the temperature loss of the flue gases of each experiment have been included in the table. The relative errors have been calculated using Eq. (16). The vast majority of the simulated thermoelectric generations stay within the expanded uncertainty interval calculated using Eq. (11-15), as Table 2 presents. The cells of the simulated thermoelectric generations that stay within their uncertainty interval are colored in green. The relative errors of the thermoelectric generation committed by the computational model can be consulted in Table 2 and Figure 13. Figure 13 a) presents the computationally obtained $\dot{W}_{TEM}$ versus the experimental values. As it can be seen most of the values stay within a ±12 %. The relative errors have been statistically studied. These errors follow a normal distribution, as it can be seen at the normal probability plot of Figure 13 b). The standard kurtosis and skewness are within the normality range (±2), specifically these values are -0.48 and 0.53 respectively. The mean of the relative error is -0.5.

$$Relative\ error = \frac{Value_{sim} - Value_{exp}}{Value_{exp}} \times 100 \qquad (16)$$

Variables			**$\dot{W}_{TEM}$ (W)**				**ΔT_{smoke} (ºC)**			**Efficiency**
$\dot{m}_{gas}\left(\frac{kg}{h}\right)$	**T_{en} (ºC)**	**R_L (Ω)**	**EXP**	**INTERVAL**	**SIM**	**ERROR (%)**	**EXP**	**SIM**	**ERROR (%)**	**η_{TEM}**
100	490	1.1	11.83	(10.19; 13.47)	11.21	-5.22	77.62	81.2	4.67	0.85
100	490	2.2	14.97	(13.34; 16.61)	15.92	6.32	78.13	80.7	3.28	1.22
100	490	4.7	14.79	(13.15; 16.42)	17.73	19.93	77.97	81.0	3.86	1.38
100	525	1.1	14.15	(12.52; 15.79)	11.95	-15.56	84.6	86.3	1.98	0.86
100	525	2.2	17.51	(15.87; 19.14)	16.80	-4.03	84	85.2	1.48	1.24
100	525	4.7	17.73	(16.10; 19.37)	19.13	7.87	85.7	86.1	0.41	1.42
100	560	1.1	15.60	(13.96; 17.24)	12.53	-19.69	92.4	90.2	-2.39	0.87
100	560	2.2	20.73	(19.09; 22.36)	18.17	-12.36	92	89.6	-2.58	1.28
100	560	4.7	20.81	(19.18; 22.49)	20.71	-0.48	92.7	90.8	-2.03	1.47
133	490	1.1	12.93	(11.29; 14.56)	12.03	-6.94	62	65.9	6.29	0.79
133	490	2.2	16.71	(15.07; 18.34)	17.33	3.73	62.7	66.8	6.53	1.15
133	490	4.7	16.84	(15.21; 18.48)	19.69	16.90	62.6	65.5	4.57	1.32
133	525	1.1	14.75	(13.11;16.38)	14.07	-4.60	77.5	76.5	-1.29	0.85
133	525	2.2	19.59	(17.96; 21.23)	20.06	2.37	77	76.1	-1.12	1.23
133	525	4.7	19.38	(17.74; 21.02)	22.65	16.84	77	75.9	-1.46	1.41
133	560	1.1	17.47	(15.51; 19.44)	15.53	-11.13	84.8	80.2	-5.48	0.89
133	560	2.2	22.97	(21.33; 24.60)	22.25	-3.14	83.5	77.4	-7.33	1.29
133	560	4.7	23.00	(20.80; 25.21)	25.14	9.29	85.4	79.9	-6.49	1.47
170	490	1.1	13.61	(11.98; 15.25)	11.98	-12.01	54.7	57.4	4.89	0.70
170	490	2.2	18.48	(16.84; 20.12)	17.78	-3.79	55.9	58.1	3.87	1.04
170	490	4.7	18.80	(17.16; 20,44)	19.99	6.34	55.4	58.3	5.21	1.18
170	525	1.1	16.69	(15.05; 18.32)	15.09	-9.54	70	67.8	-3.11	0.79
170	525	2.2	21.70	(20.06; 23.33)	21.20	-2.29	69.5	67.7	-2.66	1.13
170	525	4.7	21.63	(19.50; 23.76)	23.59	9.05	68.6	67.7	-1.31	1.28
170	560	1.1	17.89	(16.25; 19.52)	16.94	-5.29	82.6	75.1	-9.07	0.83
170	560	2.2	24.20	(22.57; 25.84)	23.38	-3.39	83.4	75.7	-9.25	1.17
170	560	4.7	24.59	(22.79; 26.39)	26.39	7.30	83.3	75.5	-9.32	1.34

Table 2. Experimental and simulated values of thermoelectric generation and the temperature loss of the flue gases.

The expanded uncertainty of the temperature loss of the flue gases (ΔT_{smoke}) has also been computed, in all the cases the value of this parameter is: $U = \pm 3.49$ ºC. The relative errors of the temperature loss of the flue gases stay within the ±10 %. The temperature loss of the flue gases is a very important parameter to take into account, especially in waste heat harvesting TEGs. As the figures show in Table 2, the computational model developed simulates the temperature loss of the gases, a key factor to obtain accurate thermoelectric generations. The temperature loss of the flue gases in the studied cases stands between 55.4 and 92.7 ^{o}C.

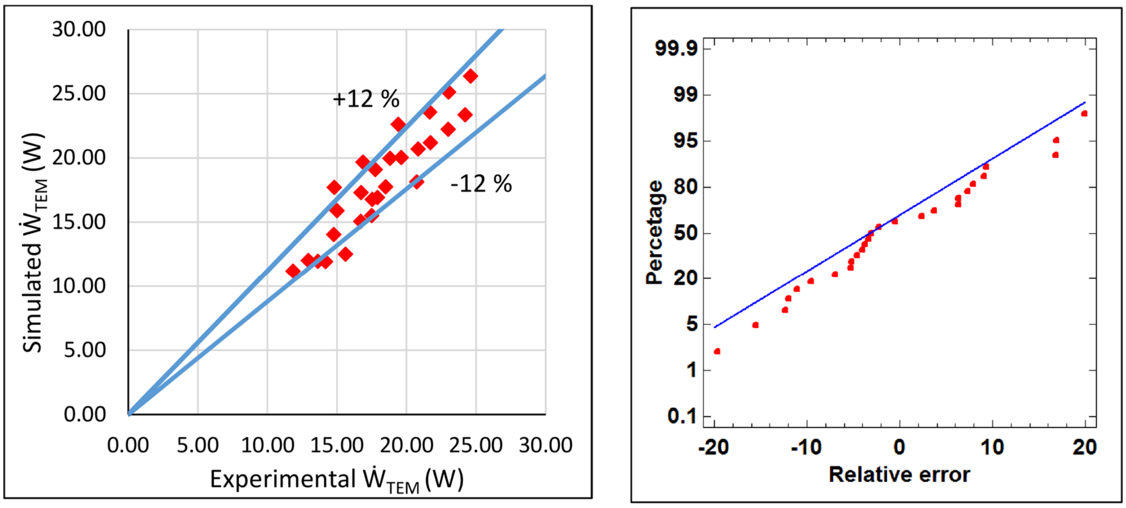

a) b)

Figure 13. Relative errors of the thermoelectric generation, a) comparison between the simulated and experimental thermoelectric generations, b) normal probability plot of the errors

The temperature difference between the sides of the TEMs determine the thermoelectric generation, hence the simulated values need to match the experimental data. The temperature of the flue gases diminishes as they flow along the chimney, the fact that the computational model contemplates, hence it has been differentiated between the difference in temperature of the TEMs between the lower and upper level. Table 3 presents the simulated values of the temperature difference at the TEMs (ΔT_{TEM}^{sim}) and the experimental ones (ΔT_{TEM}^{exp}) of nine scenarios which correspond to the extremes and the center. Three factors with three levels have been modified during the tests, thus the extremes (minimum and maximum values of the factors) and the center point represent the rest of the data. The experimental data has been obtained computing the mean and the expanded uncertainty of all the temperature probes of each level, a total of 16, 8 obtaining the hot temperature and 8 measuring the cold one. As it can be seen, most of the simulated difference in temperatures fit within the experimental intervals, the ones that do not fit correspond to the outliers in thermoelectric generation.

$\dot{m}_{gas}$ (kg/h)	T_{en} (ºC)	R_L (Ω)	First level			Second level		
			ΔT_{TEM}^{exp} (ºC)	INTERVAL	ΔT_{TEM}^{sim} (ºC)	ΔT_{TEM}^{exp} (ºC)	INTERVAL	ΔT_{TEM}^{sim} (ºC)
100	490	1.1	40.18	(33.75; 46.61)	34.27	36.67	(31.99; 41.35)	32.18
100	490	4.7	50.6	(46.23; 54.97)	45.55	45.11	(42.12; 48.1)	42.19
100	560	1.1	49.62	(44.55; 54.69)	37.3	46.27	(42.56; 49.98)	34.4
100	560	4.7	53.9	(48.24; 59.56)	49.95	48.23	(43.54;52.92)	45.73
133	525	2.2	53.47	(48.2; 58.74)	49.15	48.68	(44.47; 52.89)	44.94
170	490	1.1	48.52	(43.38; 53.65)	43.99	45	(41.28; 48.72)	41.11
170	490	4.7	56.21	(50.88; 61.53)	58.91	51.32	(47.39; 55.25)	54.66
170	560	1.1	56.9	(50.88; 62.92)	53.6	48.91	(45.67; 52.15)	47.97
170	560	4.7	64.45	(58.61; 70.29)	69.42	56.72	(51.53; 61.90)	61.81

Table 3. Experimental and simulated values of the temperature difference between the sides of the TEMs.

The computational methodology obtains accurate thermoelectric generations, especially for waste heat harvesting applications where the temperature loss of the flue gases is a vital parameter to bear in mind to get accurate thermoelectric generations. Ignoring some outliers that appear at the experimentation, it can be concluded that the accuracy of the computational model is the ±12 %. Once the computational model has been validated, it can be used to obtain other parameters, such as the efficiency of the TEMs, as Table 2 presents. As it can be seen, the efficiency is a function of the temperature and mass flow of the flue gases, and it also depends on the load resistance.

$$\eta_{TEM} = \frac{\dot{W}_{TEM}}{\dot{Q}_{TEM}} \times 100 \quad (16)$$

Therefore, this general model can predict the thermoelectric generation of any application, but it has been specifically modified to simulate the generation of waste heat harvesting applications, where the temperature drop of the heat source along the TEG is a parameter to consider into the simulation.

5. Conclusions

Applications which present waste heat are the perfect scenario for TEGs. Thermoelectric generation can take advantage of low-temperature grade heat to produce electric power, as it has been demonstrated from the designed and built prototype which is located at the exhaust of a combustion chamber which heats up water. The prototype has been divided into two levels displayed along the flow direction and composed by 16 TEMs respectively. The upper level produces a 65 % less power than the lower one, noting the importance of accounting for the temperature drop of the flue gases while they flow along the TEG. A maximum total generation of 24.59 W was obtained under the maximum temperature and mass flow tested of the flue gases, 560 ºC and 170 kg/h respectively. The reduction of the temperature to 525 ºC or the reduction in mass flow to 133 kg/h produce decreasings in the thermoelectric generation of the 11 and 6 % respectively.
This experimentation has been used to validate a general computational methodology which innovatively considers the temperature drop of the heat source as an essential parameter to simulate the thermoelectric generation of waste heat harvesting applications. The relative error of the thermoelectric generation prediction of the model stays within the ±12 %.

Acknowledgments

The authors are indebted to the Spanish Ministry of Economy and Competitiveness for the economic support to this work, included in the DPI2014-53158-R research project.

References

[1] Rattner AS, Garimella S. Energy harvesting, reuse and upgrade to reduce primary energy usage in the USA. Energy 2011;36:6172–83. doi:10.1016/j.energy.2011.07.047.

[2] Torío H, Schmidt D. Development of system concepts for improving the performance of a waste heat district heating network with exergy analysis. Energy Build 2010;42:1601–9. doi:10.1016/j.enbuild.2010.04.002.

[3] Law R, Harvey A, Reay D. Opportunities for low-grade heat recovery in the UK food processing industry. Appl Therm Eng 2013;53:188–96. doi:10.1016/j.applthermaleng.2012.03.024.

[4] Patil A, Ajah A, Herder P. Recycling industrial waste heat for sustainable district heating: A multi-actor perspective. Int J Environ Technol Manag 2009;10:412–26. doi:10.1504/IJETM.2009.023743.

[5] Rowe DM, Min G. Evaluation of thermoelectric modules for power generation. J Power Sources 1998;73:193–8. doi:10.1016/S0378-7753(97)02801-2.

[6] Qiu K, Hayden ACS. Development of thermoelectric self-powered heating equipment. J Electron Mater 2011;40:606–10. doi:10.1007/s11664-010-1473-0.

[7] Rowe DM. CRC Handbook of Thermoelectrics. New York 1995;16:1251–6. doi:10.1016/S0960-1481(98)00512-6.

[8] Hsu C-T, Yao D-J, Ye K-J, Yu B. Renewable energy of waste heat recovery system for automobiles. J Renew Sustain Energy 2010;2. doi:10.1063/1.3289832.

[9] Champier D. Thermoelectric generators: A review of applications. Energy Convers Manag 2017;140:167–81. doi:10.1016/j.enconman.2017.02.070.

[10] Singh DV, Pedersen E. A review of waste heat recovery technologies for maritime applications. Energy Convers Manag 2016;111:315–28.

doi:10.1016/j.enconman.2015.12.073.

[11] Brazdil M, Pospisil J. Thermoelectric power generation utilizing the waste heat from a biomass boiler. J Electron Mater 2013;42:2198–202. doi:10.1007/s11664-013-2570-7.

[12] Kim TY, Negash AA, Cho G. Waste heat recovery of a diesel engine using a thermoelectric generator equipped with customized thermoelectric modules. Energy Convers Manag 2016;124:280–6. doi:10.1016/j.enconman.2016.07.013.

[13] Sasaki K, Horikawa D, Goto K. Consideration of Thermoelectric Power Generation by Using Hot Spring Thermal Energy or Industrial Waste Heat. J Electron Mater 2014;44:391–8. doi:10.1007/s11664-014-3189-z.

[14] Kuroki T, Murai R, Makino K, Nagano K, Kajihara T, Kaibe H, et al. Research and Development for Thermoelectric Generation Technology Using Waste Heat from Steelmaking Process. J Electron Mater 2015;44:2151–6. doi:10.1007/s11664-015-3722-8.

[15] Araiz M, Martínez A, Astrain D, Aranguren P. Experimental and computational study on thermoelectric generators using thermosyphons with phase change as heat exchangers. Energy Convers Manag 2017;137:155–64. doi:10.1016/j.enconman.2017.01.046.

[16] Fairbanks JW. Annual merit review and peer evaluation meeting, Washington, DC. 2013. http://www.annualmeritreview.energy.gov/.

[17] Love ND, Szybist JP, Sluder CS. Effect of heat exchanger material and fouling on thermoelectric exhaust heat recovery. Appl Energy 2012;89:322–8. doi:10.1016/j.apenergy.2011.07.042.

[18] Meng JH, Wang XD, Chen WH. Performance investigation and design optimization of a thermoelectric generator applied in automobile exhaust waste

heat recovery. Energy Convers Manag 2016;120:71–80. doi:10.1016/j.enconman.2016.04.080.

[19] Rowe DM, Smith J, Thomas G, Min G. Weight penalty incurred in thermoelectric recovery of automobile exhaust heat. J Electron Mater 2011;40:784–8. doi:10.1007/s11664-011-1571-7.

[20] Wang Y, Li S, Zhang Y, Yang X, Deng Y, Su C. The influence of inner topology of exhaust heat exchanger and thermoelectric module distribution on the performance of automotive thermoelectric generator. Energy Convers Manag 2016;126:266–77. doi:10.1016/j.enconman.2016.08.009.

[21] Nguyen NQ, Pochiraju K V. Behavior of thermoelectric generators exposed to transient heat sources 2013;51:1–9. doi:10.1016/j.applthermaleng.2012.08.050.

[22] Meng F, Chen L, Sun F. Effects of temperature dependence of thermoelectric properties on the power and efficiency of a multielement thermoelectric generator. Int J Energy Environ 2012;3:137–50.

[23] Astrain D, Vián JG, Martínez A, Rodríguez A. Study of the influence of heat exchangers' thermal resistances on a thermoelectric generation system. Energy 2010;35:602–10. doi:10.1016/j.energy.2009.10.031.

[24] Aranguren P, Astrain D, Rodríguez A, Martínez A. Experimental investigation of the applicability of a thermoelectric generator to recover waste heat from a combustion chamber. Appl Energy 2015;152:121–30. doi:10.1016/j.apenergy.2015.04.077.

[25] Liu C, Zhong Li W. An Experimental Study of a Novel Prototype for Thermoelectric Power Generation from Vehicle Exhaust. Distrib Gener Altern Energy J 2013;28:32–48. doi:10.1080/21563306.2013.10750234.

[26] Kumar S, Heister SD, Xu X, Salvador JR. Optimization of Thermoelectric

Components for Automobile Waste Heat Recovery Systems. J Electron Mater 2015;44:3627–36. doi:10.1007/s11664-015-3912-4.

[27] Rodríguez A, Vián JG, Astrain D, Martínez A. Study of thermoelectric systems applied to electric power generation. Energy Convers Manag 2009;50:1236–43. doi:10.1016/j.enconman.2009.01.036.

[28] TG12-8-01L Power Generators | Generator Modules 2017. http://www.marlow.com/power-generators/standard-generators/tg12-8-01l.html (accessed May 17, 2017).

[29] Zhang T. Multi-parameter Optimization of a Thermoelectric Power Generator and Its Working Conditions. J Electron Mater 2017;46:14–22. doi:10.1007/s11664-016-4932-4.

[30] Reddy BVK, Barry M, Li J, Chyu MK. Mathematical modeling and numerical characterization of composite thermoelectric devices. Int J Therm Sci 2013;67:53–63. doi:10.1016/j.ijthermalsci.2012.11.004.

[31] Rohsenow WM, Hartnett JP, Cho YI. Handbook of heat transfer. 3rd ed. New York: McGraw-Hill; 1998.

[32] Coleman HW, Steele WG. Experimentation, Validation, and Uncertainty Analysis for Engineers. 3rd ed. New Jersey: John Wiley & Sons; 2009.